ADVANCED FUNCTIONAL MATERIALS

Supporting Information

for *Adv. Funct. Mater.,* DOI: 10.1002/adfm.202108244

Suppressing the Jahn–Teller Effect in Mn-Based Layered Oxide Cathode toward Long-Life Potassium-Ion Batteries

Zhitong Xiao, Fanjie Xia, Linhan Xu, Xuanpeng Wang, Jiashen Meng, Hong Wang, Xiao Zhang, Lishan Geng, Jinsong Wu, and Liqiang Mai**

Supporting Information

Suppressing the Jahn−Teller Effect in Mn-Based Layered Oxide Cathode Towards Long-Life Potassium-Ion Batteries

Zhitong Xiao, Fanjie Xia, Linhan Xu, Xuanpeng Wang, Jiashen Meng, Hong Wang, Xiao Zhang, Lishan Geng, Jinsong Wu, and Liqiang Mai**

Experimental Section

Materials synthesis: All reactants are analytical grade. The $K_{0.5}Mn_{0.9-x}Co_xFe_{0.1}O_2$ (x = 0.1, 0.2, 0.3, and 0.4) were synthesized *via* a sol-gel method according to our recent work.[1] Firstly, the aqueous solution of mixing of stoichiometric values potassium nitrate (KNO_3), manganese acetate tetrahydrate ($Mn(CH_3COO)_2{\cdot}4H_2O$), cobalt acetate tetrahydrate ($Co(CH_3COO)_2{\cdot}4H_2O$), and iron nitrate nonahydrate ($Fe(NO_3)_3{\cdot}9H_2O$) were added to aqueous solution of polyvinylpyrrolidone (PVP K90, M_w= 1 300 000) and stirred continuously for 8 h at room temperature. Then, the mixed solution was evaporated to dryness at 70 °C for 12 h and pre-decomposed at 350 °C for 2 h in air to obtain a black solid. Finally, the black solid was heated in a muffle furnace at 800 °C for 10 h in air for obtaining black products. The synthesis process of $K_{0.5}Mn_{0.6}Co_{0.2}Fe_{0.1}Mg_{0.1}O_2$ and $K_{0.5}Mn_{0.6}Co_{0.2}Fe_{0.1}Ti_{0.1}O_2$ samples is same to $K_{0.5}Mn_{0.9-x}Co_xFe_{0.1}O_2$, except added the magnesium acetate tetrahydrate ($Mg(CH_3COO)_2{\cdot}4H_2O$) or dihydroxybis(ammonium lactato)titanium(IV) ($C_6H_{18}N_2O_8Ti$) in the aqueous solution. After slowly cooled down to 100 °C, the products were transferred promptly and stored into an Ar-filled glovebox.

Characterizations: The structural information was measured with a D8 Discover X-ray diffractometer using non-monochromated Cu Kα radiation (λ = 1.5406 Å). XRD Rietveld refinement was perform by TOPAS 4.2 software. The morphology was measured by a JEOL JSM-7100F with 20 kV acceleration voltage. ICP measurement was recorded with a PerkinElmer Optima 4300DV spectrometer. TEM, HAADF-STEM, HRTEM images, and SAED patterns were collected with a JEM-2100F and a Thermo Fischer Titan G2 60-300 microscope. The elemental

mapping was conducted by an EDX-GENESIS 60S spectrometer. The STEM characterization was performed on a Thermo Fischer Titan Themis STEM with 300 kV acceleration voltage and the images were obtained by an ABF detector and a HAADF detector, respectively. XPS test was carried out on a VG MultiLab 2000 instrument. Before the test, the samples are sputtered by argon plasma with power of 2000 eV after 20 s. The X-ray absorption near edge structure of Mn K-edge were measured at beamline 4B9A of Beijing Synchrotron Radiation Facility (BSRF) in transmission mode. For the in situ XRD measurement, the in situ batteries were charged to 3.9 V and then discharged to 1.5 V (*vs.* K^+/K) at 0.05 A g^{-1}, with 2θ within range from 24° to 28° and 35° to 43.5°.

Electrochemical measurements: All the electrochemical tests were conducted using coin cells (CR2016). The working electrode was prepared by casting a mixture of active material, acetylene black and polyvinylidene fluoride (PVDF) binder with a weight ratio of 70:20:10 onto Al foil, followed by drying at 70 °C in glovebox for 10 hours. The area loading of cathode materials were approximately 1.5-2.5 mg cm^{-2}. The electrolyte was a solution of 0.8 M potassium hexafluorophosphate (KPF_6) in ethylene carbonate (EC) and diethyl carbonate (DEC) (1:1 in volume). Potassium metal foil was used as the counter electrode and porous glass microfiber filter (Grade GF/D Whatman) was used as the separator. Galvanostatic discharge/charge tests were carried out using a LAND CT2001A multichannel testing system. GITT curve was also measured using a LAND CT2001A multichannel testing system, which conducted at a pulse current of 0.03 A g^{-1} for 5 min, followed with a relaxation for 30 min. EIS and CV measurements were conducted with an Auto lab PGSTAT 302N and CHI 600e electrochemical workstation. All the electrochemical measurements were performed over a voltage range of 1.5-3.9 V at room temperature.

First-principles calculations: The present calculations were performed by using a first-principles method based on the DFT with the GGA in the form of PBE exchange-correlation functional, as implemented in the Vienna Ab initio Simulation Package (VASP).[3–5] The wave functions are expanded in plane waves up to a kinetic energy cutoff of 520 eV. The Brillouin zone (BZ) integrals were performed using a Monkhorst-Pack sampling scheme with a k-point mesh resolution of $2\pi \times 0.05$ $Å^{-1}$.[6] The unit cell lattice parameters (unit cell shape

and size) and atomic coordinates were fully relaxed in each system until the forces on all the atoms were smaller than 0.01 eV $Å^{-1}$. The DFT calculations are supplemented with Hubbard Coulomb interaction potential (U) corrections for d-electrons.[7] The U values are 5.3 eV, 3.32 eV, and 3.9 eV for Fe, Co, and Mn respectively, as provided in the Materials Project.[8]

Table S1 ICP measurement results of $K_{0.5}Mn_{0.9-x}Co_xFe_{0.1}O_2$ (x = 0.1, 0.2, 0.3, and 0.4).

Theoretical chemical formula	K: Mn: Co: Fe
$K_{0.5}Mn_{0.8}Co_{0.1}Fe_{0.1}O_2$	0.509: 0.805: 0.101: 0.100
$K_{0.5}Mn_{0.7}Co_{0.2}Fe_{0.1}O_2$	0.504: 0.706: 0.197: 0.100
$K_{0.5}Mn_{0.6}Co_{0.3}Fe_{0.1}O_2$	0.507: 0.606: 0.297: 0.100
$K_{0.5}Mn_{0.5}Co_{0.4}Fe_{0.1}O_2$	0.505: 0.493: 0.393: 0.100

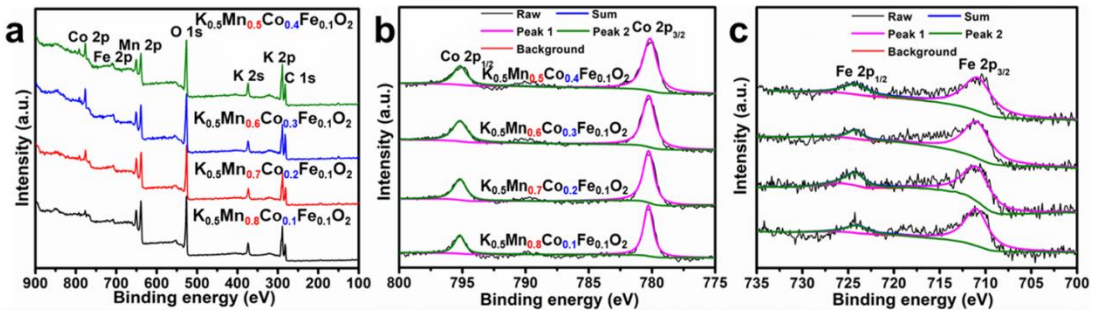

Figure S1 XPS survey spectra (a) and the corresponding spectra of Co 2p (b) and Fe 2p (c), respectively.

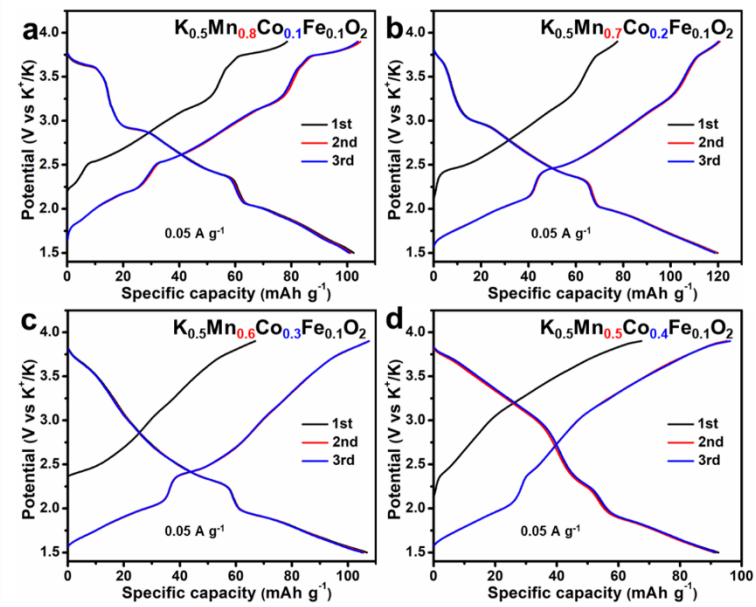

Figure S2 Charge/discharge curves (for the 1st, 2nd and 3rd cycle at 0.05 A g^{-1}) of $K_{0.5}Mn_{0.8}Co_{0.1}Fe_{0.1}O_2$ (a), $K_{0.5}Mn_{0.7}Co_{0.2}Fe_{0.1}O_2$ (b), $K_{0.5}Mn_{0.6}Co_{0.3}Fe_{0.1}O_2$ (c) and $K_{0.5}Mn_{0.5}Co_{0.4}Fe_{0.1}O_2$ (d), respectively.

Table S2 ICP measurement results of $K_{0.5}Mn_{0.9-x}Co_xFe_{0.1}O_2$ (x = 0.1, 0.2, 0.3, and 0.4) electrode before and after immersed in the potassium-contained electrolyte.

Layered oxides	K: Mn: Co: Fe (electrode **before** immersed in electrolyte)	K: Mn: Co: Fe (electrode **after** immersed in electrolyte)
$K_{0.5}Mn_{0.8}Co_{0.1}Fe_{0.1}O_2$	0.507: 0.807: 0.104: 0.100	0.572: 0.809: 0.098: 0.100
$K_{0.5}Mn_{0.7}Co_{0.2}Fe_{0.1}O_2$	0.509: 0.703: 0.202: 0.100	0.585: 0.707: 0.203: 0.100
$K_{0.5}Mn_{0.6}Co_{0.3}Fe_{0.1}O_2$	0.508: 0.598: 0.296: 0.100	0.611: 0.609: 0.308: 0.100
$K_{0.5}Mn_{0.5}Co_{0.4}Fe_{0.1}O_2$	0.503: 0.497: 0.395: 0.100	0.592: 0.508: 0.406: 0.100

For sample preparation, the electrodes were immersed in the potassium-contained electrolyte (0.8 M KPF_6 in EC and DEC (1:1 in volume)) for 6 h. Then the test samples were harvested *via* washed with DEC and ethanol several times, before being dried at room temperature in argon atmosphere filled glove box.

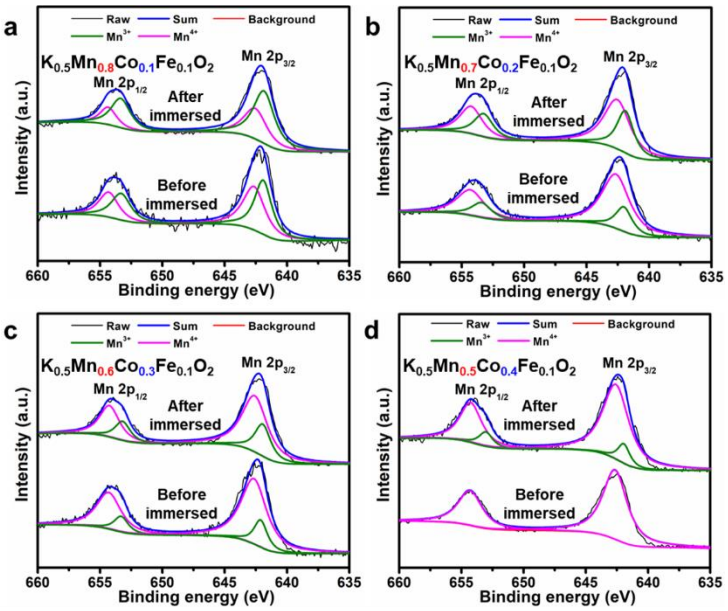

Figure S3 XPS spectra of Mn 2p for $K_{0.5}Mn_{0.9-x}Co_xFe_{0.1}O_2$ (x = 0.1, 0.2, 0.3, and 0.4) electrode before and after immersed in the potassium-contained electrolyte.

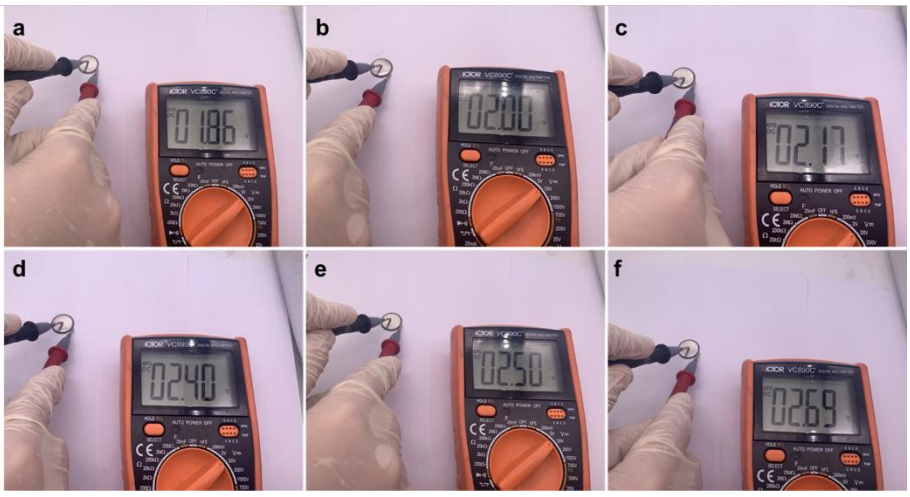

Figure S4 Photograph of the open-circuit voltage for $K_{0.5}Mn_{0.7}Co_{0.2}Fe_{0.1}O_2$ batteries before electrochemical testing.

The measured batteries used the same batch of electrode, the same electrolyte, electrolyte addition and potassium metal foil. The batteries were also placed for the same time before the measurement.

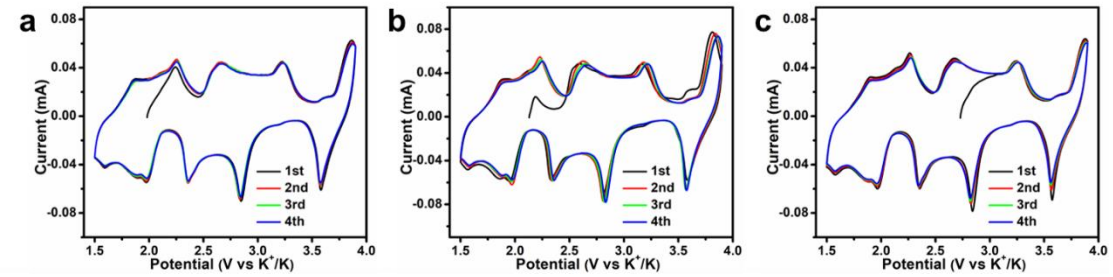

Figure S5 CV curves of $K_{0.5}Mn_{0.8}Co_{0.1}Fe_{0.1}O_2$ measured with the different open-circuit voltage.

The possible mismatch between the average valence state and electrochemical test results can be attributed to the following reasons: First, the valence states of the elements in the active material are not affected when the active material mixed with acetylene black and binder to fabricated the electrode. However, when the electrode is immersed in the potassium-contained electrolyte, the K^+ in the electrolyte is spontaneously intercalated in the K layer of active material, which is proved by ICP measurement (Table S2). This phenomenon is attributed to the deficiency of K in layered oxides caused by large ion radius of K^+, which is widely reported in K-contained layered oxide materials.[9-13] With the insertion of K^+, the valence state of Mn is decreased due to the charge compensation mechanism. The XPS results of electrode materials before and after immersed in the potassium-contained electrolyte demonstrated this process (Figure S3).

Second, during the battery assembly process, the open-circuit voltage of the battery is affected by many uncontrollable factors, such as assembly technology, self-discharge during placement, *etc.* (Figure S4). However, the open-circuit voltage of the battery has a considerable influence on the initial charging process in the CV test (Figure S5). When the open-circuit voltage is low, the oxidation peaks in the low voltage region can appear in the initial CV curve. In contrast, when the open-circuit voltage is high, these oxidation peaks are not appeared. The result of the electrochemical test cannot objectively and truly reflect the initial valence state of the material.[14-16] Therefore, the comprehensive analysis of the whole charge and discharge process is more significant.

Table S3 ICP measurement results of $K_{0.5}Mn_{0.6}Co_{0.2}Fe_{0.1}Ti_{0.1}O_2$ and $K_{0.5}Mn_{0.6}Co_{0.2}Fe_{0.1}Mg_{0.1}O_2$.

Theoretical chemical formula	K: Mn: Co: Fe: Mg/Ti
$K_{0.5}Mn_{0.6}Co_{0.2}Fe_{0.1}Ti_{0.1}O_2$	0.506: 0.608: 0.195: 0.100: 0.997
$K_{0.5}Mn_{0.6}Co_{0.2}Fe_{0.1}Mg_{0.1}O_2$	0.504: 0.607: 0.202: 0.100: 0.992

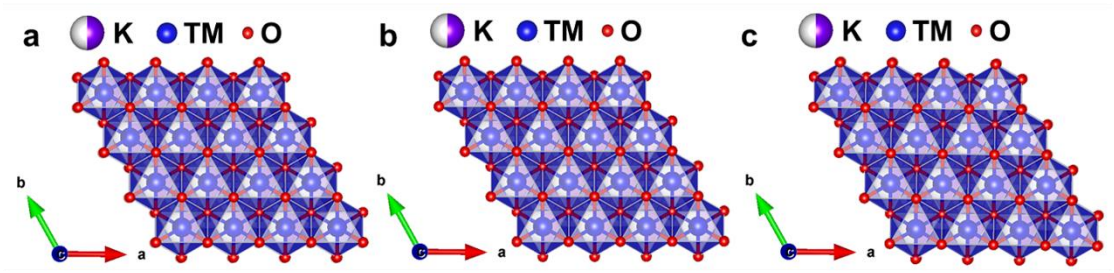

Figure S6 Schematic illustration of $K_{0.5}Mn_{0.7}Co_{0.2}Fe_{0.1}O_2$ (a), $K_{0.5}Mn_{0.6}Co_{0.2}Fe_{0.1}Ti_{0.1}O_2$ (b) and $K_{0.5}Mn_{0.6}Co_{0.2}Fe_{0.1}Mg_{0.1}O_2$ (c), respectively, crystal viewed along the [001] zone axis.

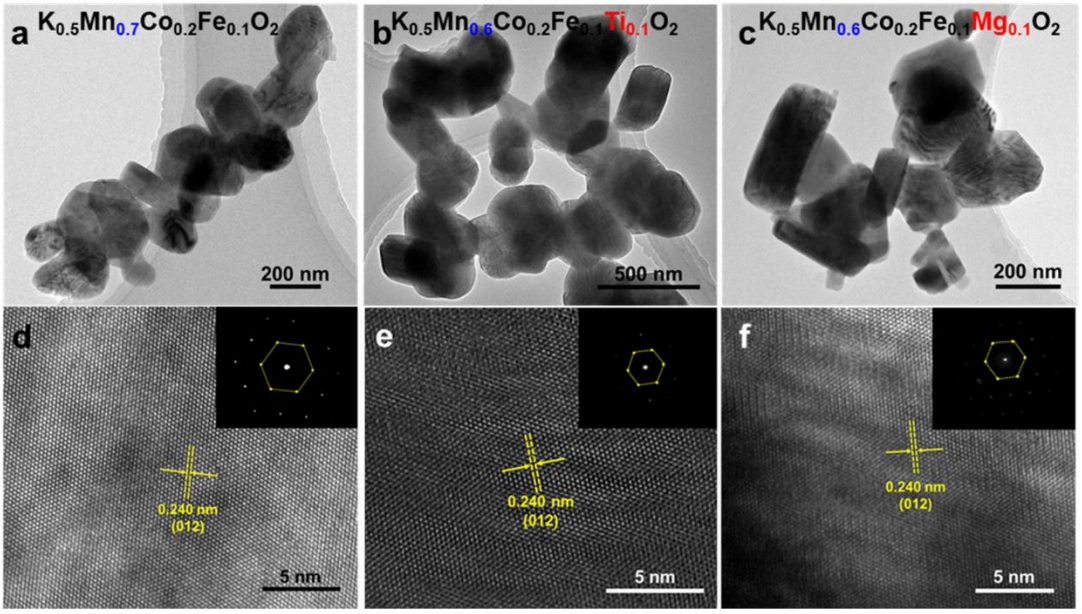

Figure S7 TEM (a-c) and HRTEM (d-f) images (inset: SAED pattern) of $K_{0.5}Mn_{0.7}Co_{0.2}Fe_{0.1}O_2$, $K_{0.5}Mn_{0.6}Co_{0.2}Fe_{0.1}Ti_{0.1}O_2$ and $K_{0.5}Mn_{0.6}Co_{0.2}Fe_{0.1}Mg_{0.1}O_2$, respectively.

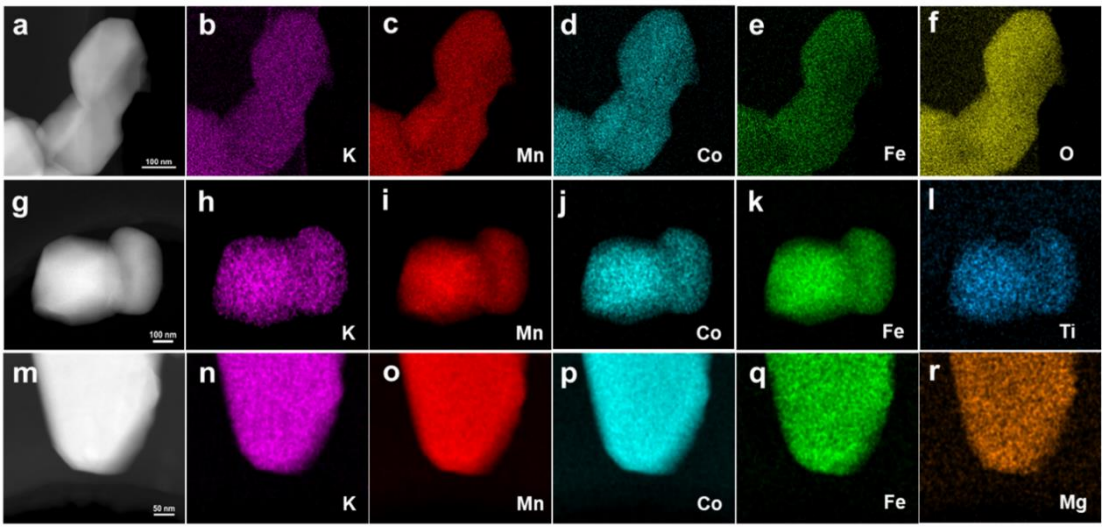

Figure S8 (a-f) HAADF-STEM image of $K_{0.5}Mn_{0.7}Co_{0.2}Fe_{0.1}O_2$ and the corresponding EDS mappings for K, Mn, Co, Fe, and O elements. (g-l) HAADF-STEM image of $K_{0.5}Mn_{0.6}Co_{0.2}Fe_{0.1}Ti_{0.1}O_2$ and the corresponding EDS mappings for K, Mn, Co, Fe, and Ti elements. (m-r) HAADF-STEM image of $K_{0.5}Mn_{0.6}Co_{0.2}Fe_{0.1}Mg_{0.1}O_2$ and the corresponding EDS mappings for K, Mn, Co, Fe, and Mg elements.

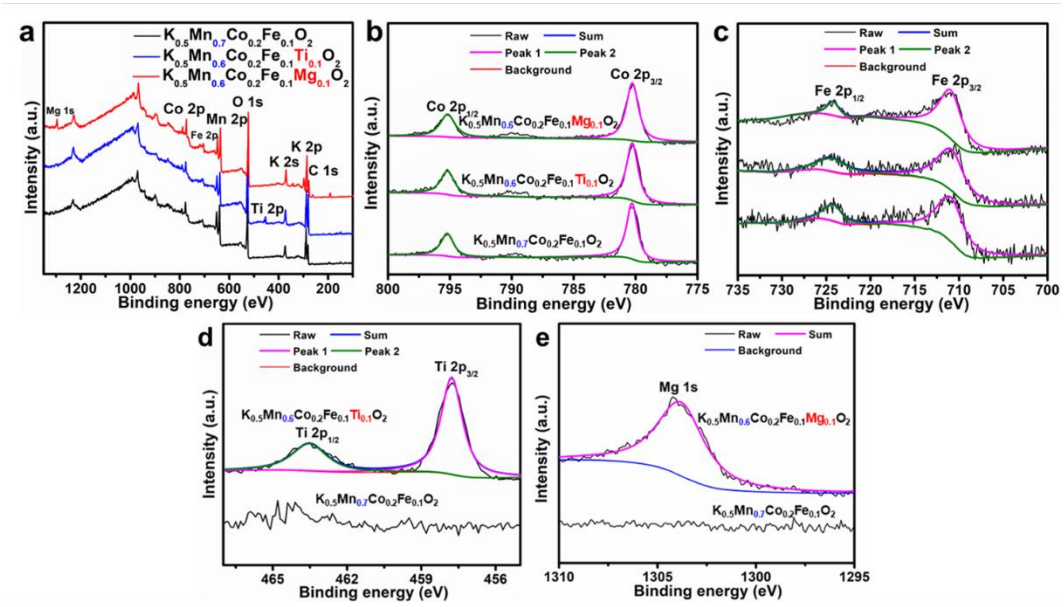

Figure S9 XPS survey spectra (a) and the corresponding spectra of Co 2p (b), Fe 2p (c), Ti 2p (d) and Mg 1s (e), respectively, for $K_{0.5}Mn_{0.7}Co_{0.2}Fe_{0.1}O_2$, $K_{0.5}Mn_{0.6}Co_{0.2}Fe_{0.1}Ti_{0.1}O_2$ and $K_{0.5}Mn_{0.6}Co_{0.2}Fe_{0.1}Mg_{0.1}O_2$.

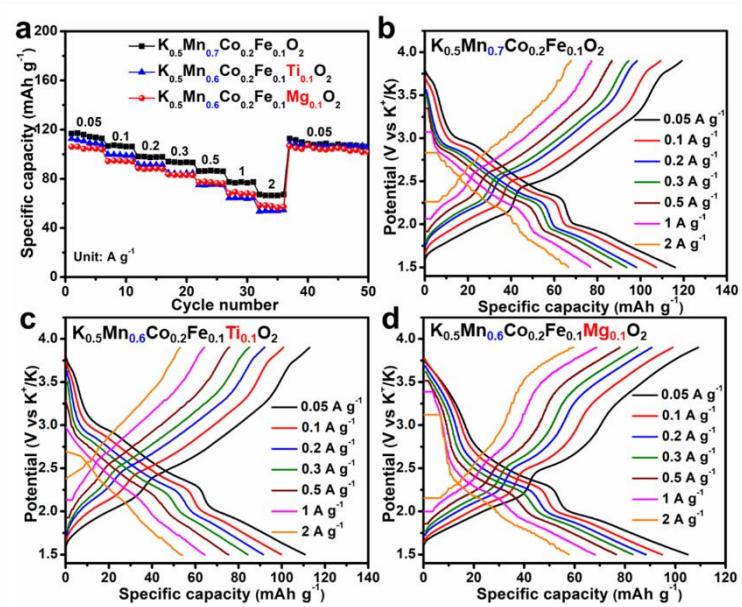

Figure S10 Rate performance conducted at 0.05, 0.1, 0.2, 0.3, 0.5, 1, 2, and back to 0.05 A g^{-1} (a); the corresponding discharge/charge curves of rate performance for $K_{0.5}Mn_{0.7}Co_{0.2}Fe_{0.1}O_2$ (b) $K_{0.5}Mn_{0.6}Co_{0.2}Fe_{0.1}Ti_{0.1}O_2$ (c) and $K_{0.5}Mn_{0.6}Co_{0.2}Fe_{0.1}Mg_{0.1}O_2$ (d), respectively.

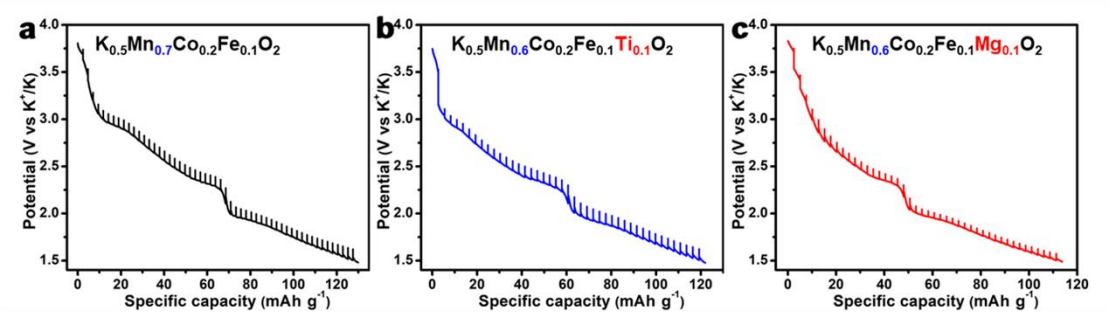

Figure S11 Potential response of $K_{0.5}Mn_{0.7}Co_{0.2}Fe_{0.1}O_2$ (a), $K_{0.5}Mn_{0.6}Co_{0.2}Fe_{0.1}Ti_{0.1}O_2$ (b) and $K_{0.5}Mn_{0.6}Co_{0.2}Fe_{0.1}Mg_{0.1}O_2$ (c), respectively, during GITT measurement.

Table S4 Structural parameters and atomic position of $K_{0.5}Mn_{0.7}Co_{0.2}Fe_{0.1}O_2$ from Rietveld refinement.

Formula			$K_{0.5}Mn_{0.7}Co_{0.2}Fe_{0.1}O_2$		
Crystal system			Hexagonal		
Space group			*R3m*		
Atom	*x*	*y*	*z*	Occupancy	Thermal factor
K	0	0	0.8312	0.5	0.02995
Mn	0	0	0	0.7	0.06412
Co	0	0	0	0.2	0.06412
Fe	0	0	0	0.1	0.06412
O	0	0	0.3822	1.0	0.28403
O	0	0	0.6294	1.0	0.03207
$a = b$ (Å)			2.8792(1)		
c (Å)			21.0051(5)		
Cell volume ($Å^3$)			150.802(11)		
Crystal density (g cm^{-3})			3.547		
R_{wp} (%)			6.33		
R_p (%)			5.00		
x^2			1.754		

Table S5 Structural parameters and atomic position of $K_{0.5}Mn_{0.6}Co_{0.2}Fe_{0.1}Ti_{0.1}O_2$ from Rietveld refinement.

Formula			$K_{0.5}Mn_{0.6}Co_{0.2}Fe_{0.1}Ti_{0.1}O_2$		
Crystal system			Hexagonal		
Space group			*R3m*		
Atom	*x*	*y*	*z*	Occupancy	Thermal factor
K	0	0	0.8312	0.5	0.03000
Mn	0	0	0	0.6	0.06410
Co	0	0	0	0.2	0.06410
Fe	0	0	0	0.1	0.06410
Ti	0	0	0	0.1	0.06410
O	0	0	0.3822	1.0	0.28400
O	0	0	0.6294	1.0	0.03210
$a = b$ (Å)			2.8861(2)		
c (Å)			20.9790(8)		
Cell volume (Å^3)			151.339(22)		
Crystal density (g cm^{-3})			3.511		
R_{wp} (%)			7.28		
R_p (%)			5.35		
x^2			2.4		

Table S6 Structural parameters and atomic position of $K_{0.5}Mn_{0.6}Co_{0.2}Fe_{0.1}Mg_{0.1}O_2$ from Rietveld refinement.

Formula			$K_{0.5}Mn_{0.6}Co_{0.2}Fe_{0.1}Mg_{0.1}O_2$		
Crystal system			Hexagonal		
Space group			*R3m*		
Atom	*x*	*y*	*z*	Occupancy	Thermal factor
K	0	0	0.8312	0.5	0.02717
Mn	0	0	0	0.6	0.06777
Co	0	0	0	0.2	0.06777
Fe	0	0	0	0.1	0.06777
Mg	0	0	0	0.1	0.06777
O	0	0	0.3822	1.0	0.36468
O	0	0	0.6294	1.0	0.00633
$a = b$ (Å)			2.8836(1)		
c (Å)			20.9145(8)		
Cell volume ($Å^3$)			150.607(13)		
Crystal density (g cm^{-3})			3.450		
R_{wp} (%)			6.77		
R_p (%)			4.91		
x^2			1.91		

Table S7 Electrochemical performance comparison of P3-type $K_{0.5}Mn_{0.6}Co_{0.2}Fe_{0.1}Mg_{0.1}O_2$ with previously reported layered oxide cathodes in PIBs.

Layered oxides cathode	Voltage range (V)	Discharge capacity [mAh g^{-1}]/current density [mA g^{-1}]	Cycling performance capacity retention (%)/cycles	Rate capability [mAh g^{-1}]/current density [mA g^{-1}]	Ref
P3-type $K_{0.5}Mn_{0.6}Co_{0.2}Fe_{0.1}Mg_{0.1}O_2$	**1.5-3.9**	**106.1/50**	**91/150**	**57.8/2000**	**Our work**
P3-type $K_{0.5}MnO_2$	1.5-3.9	106/5	70/50	38/300	S17
$K_{0.45}Mn_{0.8}Fe_{0.2}O_2$	1.5-4.0	106.2/20	77.3/100	64.9/200	S14
P3-type $K_{0.54}Co_{0.5}Mn_{0.5}O_2$	1.5-3.9	120.4/20	85/100	78/500	S11
P2-type $K_{0.44}Ni_{0.22}Mn_{0.78}O_2$	1.5-4.0	125.5/10	80/30	58/500	S12
P2-type $K_{0.75}Ni_{1/3}Mn_{2/3}O_2$	1.5-4.3	110/20	86/300	91/1400	S18
P3-type $K_{0.5}Mn_{0.72}Ni_{0.15}Co_{0.13}O_2$	1.5-4.0	82.5/10	85/100	57.9/500	S19
P3-type $K_{0.45}Ni_{0.1}Co_{0.1}Al_{0.05}Mn_{0.75}O_2$	1.5-4.0	84.5/20	76.1/100	37/500	S15
P2-type $K_{0.75}Mn_{0.8}Ni_{0.1}Fe_{0.1}O_2$	1.5-3.9	110/10	70/200	62.7/1000	S20

References

[1] Z. Xiao, J. Meng, F. Xia, J. Wu, F. Liu, X. Zhang, L. Xu, X. Lin, L. Mai, *Energy Environ. Sci.* **2020**, *13*, 3129.

[2] J. P. Perdew, K. Burke, M. Ernzerhof, *Phys. Rev. Lett.*, **1996**, *77*, 3865.

[3] G. Kresse, J. Furthmüller, *Phys. Rev. B*, **1996**, *54*, 11169.

[5] G. Kresse, J. Furthmüller, *Comput. Mater. Sci.*, **1996**, *6*, 15.

[6] H. J. Monkhorst, J. D. Pack, *Phys. Rev. B*, **1976**, *13*, 5188.

[7] S. Dudarev, G. Botton, S. Savrasov, C. Humphreys, A. Sutton, *Phys. Rev. B*, **1998**, *57*, 1505.

[8] A. Jain, S. P. Ong, G. Hautier, W. Chen, W. D. Richards, S. Dacek, S. Cholia, D. Gunter, D. Skinner, G. Ceder, K. A. Persson, *APL Mater.*, **2013**, *1*, 011002.

[9] H. Kim, J. C. Kim, S.-H. Bo, T. Shi, D.-H. Kwon, G. Ceder, *Adv. Energy Mater.* **2017**, *7*, 1700098.

[10] T. Deng, X. Fan, C. Luo, J. Chen, L. Chen, S. Hou, N. Eidson, X. Zhou, C. Wang, *Nano Lett.* **2018**, *18*, 1522.

[11] J. U. Choi, J. Kim, J.-Y. Hwang, J. H. Jo, Y.-K. Sun, S.-T. Myung, *Nano Energy* **2019**, *61*, 284.

[12] L. Deng, T. Wang, Y. Hong, M. Feng, R. Wang, J. Zhang, Q. Zhang, J. Wang, L. Zeng, Y. Zhu, L. Guo, *ACS Energy Lett.* **2020**, *5*, 1916.

[13] X. Zhang, Y. Yang, X. Qu, Z. Wei, G. Sun, K. Zheng, H. Yu, F. Du, *Adv. Funct. Mater.* **2019**, *29*, 1905679.

[14] C. Liu, S. Luo, H. Huang, X. Liu, Y. Zhai, Z. Wang, *Chem. Eng. J.* **2019**, *378*, 122167.

[15] R. Dang, N. Li, Y. Yang, K. Wu, Q. Li, Y. L. Lee, X. Liu, Z. Hu, X. Xiao, *J. Power Sources* **2020**, *464*, 228190.

[16] L. Liu, J. Liang, W. Wang, C. Han, Q. Xia, X. Ke, J. Liu, Q. Gu, Z. Shi, S. Chou, *ACS Appl. Mater. Interfaces* **2021**, *13*, 28369.

[17] H. Kim, D. H. Seo, J. C. Kim, S. H. Bo, L. Liu, T. Shi, G. Ceder, *Adv. Mater.* **2017**, *29*, 1702480.

[18] J. H. Jo, J. U. Choi, Y. J. Park, Y. H. Jung, D. Ahn, T. Y. Jeon, H. Kim, J. Kim, S. T.

Myung, *Adv. Energy Mater.* **2020**, *10*, 1903605.

[19] Q. Deng, F. Zheng, W. Zhong, Q. Pan, Y. Liu, Y. Li, G. Chen, Y. Li, C. Yang, M. Liu, *Chem. Eng. J.* **2020**, *392*, 123735.

[20] J.-Y. Hwang, J. Kim, T.-Y. Yu, H.-G. Jung, J. Kim, K.-H. Kim, Y.-K. Sun, *J. Mater. Chem. A* **2019**, *7*, 21362.